April 14, 2020
Volume 53
Number 7

Macromolecules

pubs.acs.org/Macromolecules

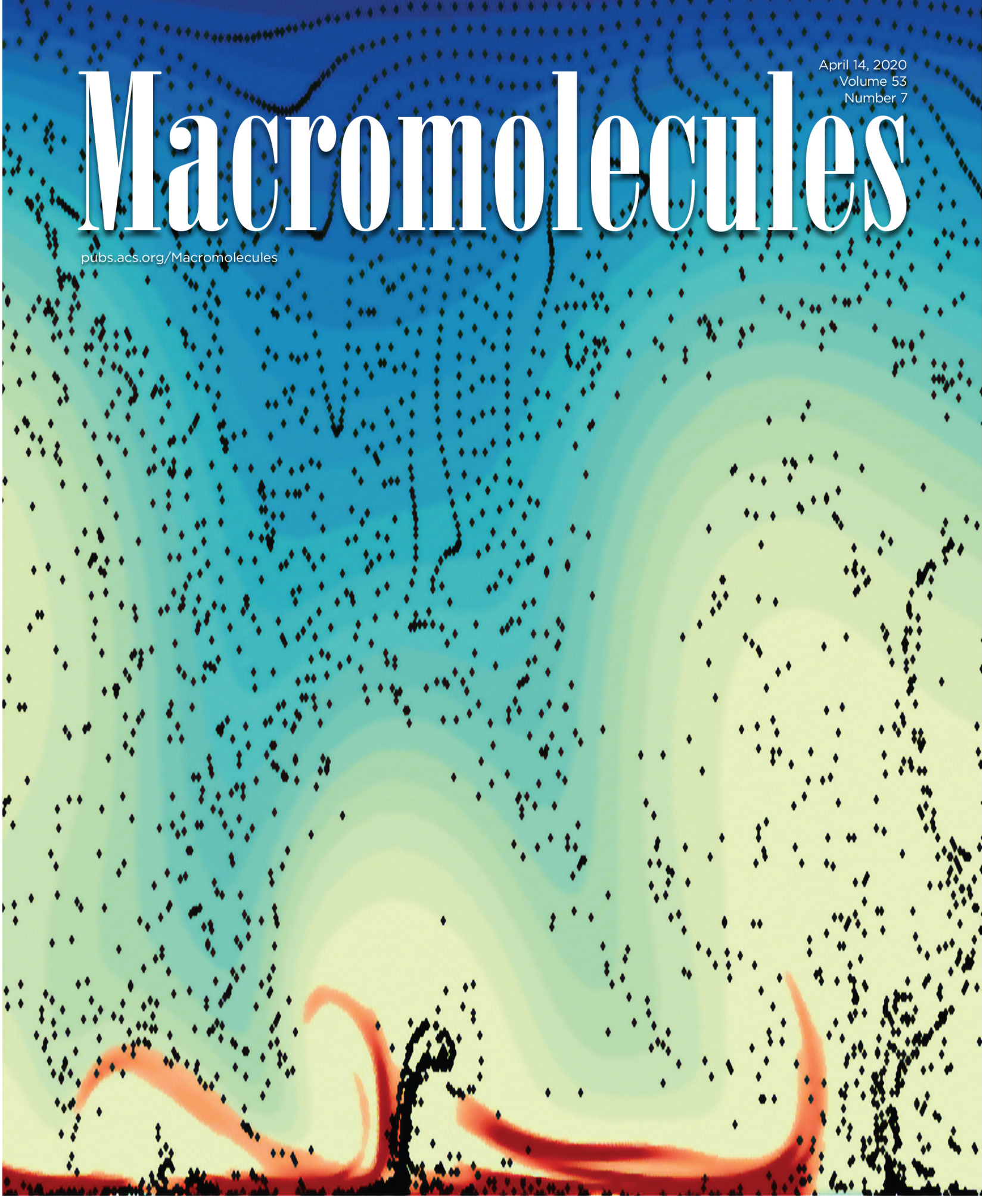

ACS Publications
Most Trusted. Most Cited. Most Read.

www.acs.org

Macromolecules

pubs.acs.org/Macromolecules Article

Electrodeposition of Zinc in Aqueous Electrolytes Containing High Molecular Weight Polymers

Duhan Zhang, Alexander J. Warren, Gaojin Li, Zhu Cheng, Xiaoxing Han, Qing Zhao, Xiaotun Liu, Yue Deng, and Lynden A. Archer*

Cite This: *Macromolecules* 2020, 53, 2694–2701 Read Online

ACCESS | Metrics & More | Article Recommendations | Supporting Information

ABSTRACT: Strong polarization of the ion distribution in liquid electrolytes subjected to potential differences exceeding the thermal voltage, $V_T = kT/e$, produces a hydrodynamic instability termed electroconvection at ion-selective interfaces. Electroconvection is desirable in some situations (e.g., electrodialysis) because it promotes mixing in a stagnant electrolyte layer, enhancing the ion flux at a fixed potential difference. It is undesirable in others (e.g., electrodeposition of metals) where early experiments show that convective fluid rolls associated with hydrodynamic instability in bounded electrolytes produce preferential metal deposition at localized regions on an electrode. Such localized deposition drives the family of morphological instabilities loosely termed dendritic electrodeposition. We experimentally investigate the effect of ultrahigh molecular weight polymer additives on the onset conditions and physical characteristics of both instabilities. Direct observations of electrodeposit morphology and tracer particle motions used in tandem with indirect electrokinetic measurements reveal that even at moderate concentrations, the polymer additives have a large beneficial effect in extending the range of electric potentials where stable electrodeposition is observed. Additionally, we report that at polymer concentrations above the entanglement threshold, high molecular weight polymers impart elasticity to liquid electrolytes which dampen electroconvective flow at a cation-selective interface but have at most a minimal effect on the bulk ionic conductivity of the liquid.

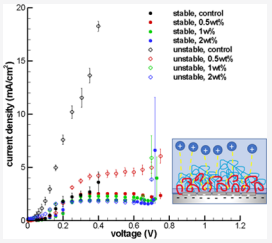

INTRODUCTION

At electric potentials above the thermal voltage, kT/e (k: Boltzmann constant,T: absolute temperature, e: elementary charge), transport of ions at an ion-selective interface can trigger electrokinetic instabilities in liquid electrolytes. At the metal electrodes used in rechargeable Zn, Mg, and Al batteries, these electrokinetic instabilities drive selective electrodeposition of the metal at specific sites on the electrode, leading to the morphological instability loosely termed dendritic electrodeposition. Dendritic electrodeposition is a nuisance in metal coating processes because it leads to a nonuniform metal finish. It is unsafe in rechargeable batteries that use metal anodes because it can cause localized, nonplanar growth of metal deposits which proliferate in the interelectrode space, internally shorting the cell. At a cation-selective interface, such as that formed by charged polymers, including polystyrene sulfonic acid or perfluorinated polyether sulfonates (*e.g.* Nafion), no deposition occurs and the electrokinetic instability manifests instead as a hydrodynamic instability termed electroconvection.

In classical electrokinetic models, hydrodynamic instability at either a metal or cation-selective interface is predicted to result from formation of an extended space charge layer (ESCL) near the negative electrode/electrolyte or membrane/electrolyte interface.[1,2] The ESCL is characterized by a depleated concentration of both negative and positive charges in the electrolyte, but because it exists near a cation-rich interface, it typically hosts a small excess of the positive charge and as a result local electroneutrality can be violated in a strongly polarized electrolyte. The thickness of the ESCL, $\Lambda_{ESCL} \approx L\left\{\left(\frac{Ve}{kT}\right)\frac{\kappa^{-1}}{L}\right\}^{2/3}$, depends on the interelectrode spacing, L, the imposed electric potential relative to the thermal voltage, $V/(kT/e)$, and the Debye screening length, κ^{-1}. In macroscopic electrochemical cells containing even moderately salty electrolyte, $\frac{L}{\kappa^{-1}} \gg \left(\frac{Ve}{kT}\right)^{-2}$, and therefore Λ_{ESCL} is generally substantially larger than the thickness of the equilibrium space charge layer ($O(\kappa^{-1})$), which forms spontaneously in any electrolyte medium near a charged substrate.

In typically studied salt-in-solvent type electrolytes used in electrochemical cells, these classical effects are complicated by density differences between the solvated ions and solvent, which produce density gradients. Depending on the relative orientations of the gravitational and electric field in such systems, the density differences can exacerbate electrokinetic

Received: January 8, 2020
Revised: March 3, 2020
Published: March 23, 2020

https://dx.doi.org/10.1021/acs.macromol.0c00037
Macromolecules 2020, 53, 2694–2701

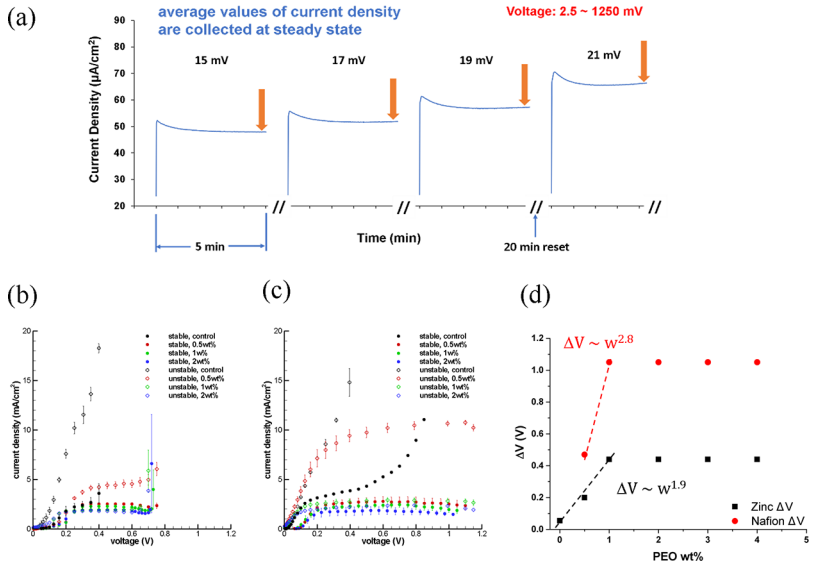

Figure 1. (a) Voltage ramp control measurement method used to determine the $J-V$ curve in liquid electrolytes. (b) $J-V$ curves for Zn||Zn cells with electrodes spaced 0.8 mm apart and containing 50 mM $ZnSO_4$ aqueous electrolyte with/without polyethylene oxide (PEO) additives. Filled symbols are from measurements taken in the gravity stable cell configuration and open symbols correspond to the gravity unstable configuration. (c) Same as (b), except that the working electrode is covered by a thick, cation-selective membrane (Nafion). (d) Effect of PEO concentration on the width of the diffusion-limited regime in Zn||Zn and Zn||Nafion cells in the gravity stable configuration.

instability by producing a downwelling of the heavier ions driving a Rayleigh−Bernard-like instability.[3−6] If the gravitational and electric fields are parallel, the ESCL is expected to grow faster and electrokinetic processes near ion-selective interfaces are more unstable. In the reverse situation, gravity has a slight stabilizing effect, leading to the designation of an electrochemical cell in which the gravitational and electrical field are antiparallel as existing in a gravity stable configuration. In either configuration, the effect of gravity can be quantified in terms of the Rayleigh number, $R_a = \frac{\Delta\rho g L^3}{\mu D}$, which quantifies the relative magnitude of the gravitational force to the viscous drag on density gradients in the electrolyte.[3] $\Delta\rho$ is the density difference between the electrolyte salt and solvent; g is the magnitude of gravitational acceleration; μ and D are, respectively, the electrolyte viscosity and diffusivity.

Here, we report on the effect of ultrahigh molecular weight polymers on the stability of electrokinetic processes in three specific contexts: (i) electrodeposition at a metal electrode, where the hydrodynamic and morphological instabilities may coexist. (ii) Ion migration in an electrolyte near a cation-selective membrane, where only the hydrodynamic instability is anticipated. And, (iii) gravity assisted versions of (i) and (ii). Aqueous zinc-based electrochemical cells are the focus of our studies for a variety of fundamental and practical reasons. From a fundamental perspective, Zn does not form a solid−electrolyte interface as does lithium and sodium used in earlier studies.[7] As a result, the electrokinetics of Zn ions near a metal electrode are more classical and as such provide a more straightforward platform for establishing behaviors that may be generalized to other systems. Additionally, because the density of the zinc sulphate ($ZnSO_4$) salt (3.54 g/cm^3) used in our studies is higher than the analogous Li salts studied previously (2.22 g/cm^3), gravitational effects will be more important and their role will be easier to isolate and study. From a practical perspective, rechargeable batteries based on Zn anodes are an area of significant scientific and technological interest,[8−15] including very recently as flow batteries that simultaneously perform an energy storage and actuation function in fully autonomous aquatic robots.[16] This interest is motivated by the high specific capacity (820 mAh/g), good air and moisture stability, and high earth-abundance of the Zn anode, as well as nontoxicity of the aqueous electrolytes used in such cells.[17−20] The relatively low electrode potential (−0.762 V vs SHE), propensity to form high-modulus dendrites at practical metal throughputs,[11−15] and the relatively low electrochemical stability window (1.23 V) of water are well-known practical hurdles for commercial Zn batteries. The key finding from the present study is that in comparison to other approaches[9−16,18,21,22] that have been reported for stabilizing the zinc anode against dendrite formation, low concentrations of ultrahigh molecular weight water-soluble polymers are very effective in suppressing dendritic electrodeposition of Zn through their specific ability to delay/arrest electroconvection.

Figure 1a summarizes the measurement procedure used to determine all current density versus voltage ($J-V$) curves reported in the study. The current response at each voltage was obtained at long-times after imposition of a sequence of voltages in a time-dependent ramp. As illustrated in the figure, at long times following each voltage step the measured current reaches a quasi-steady-state value, which we report in Figure 1b,c as the characteristic *steady-state* current density for that voltage. Voltages covering a wide range 2.5−1250 mV were investigated; the highest voltages studied are limited by electrolysis of the aqueous electrolyte solvent. Measurements were repeated at least five times at each voltage to obtain statistical information about run-to-run variability of the current response and, more fundamentally, to develop insights about the stability of the underlying electrokinetics. Because the voltage scan rate quickly falls to zero following each step, this method ensures that the diffusion boundary layer thickness at the long time points where the current is recorded exceeds the interelectrode distance L; allowing transient current contributions from double-layer rearrangement and continuous current contributions from Faradaic processes at the electrodes

https://dx.doi.org/10.1021/acs.macromol.0c00037
Macromolecules 2020, 53, 2694−2701

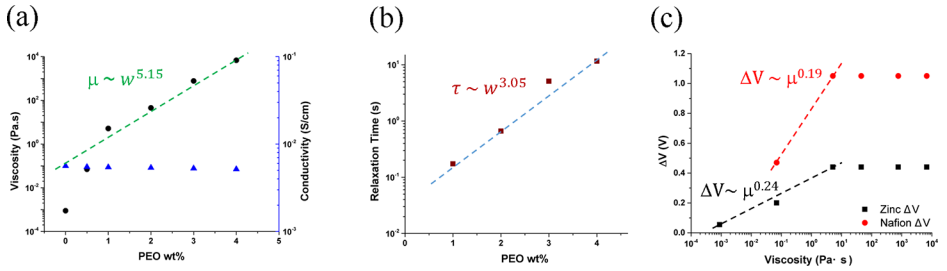

Figure 2. Physical properties of polymer solution electrolytes: (a) viscosity and ion conductivity; (b) relaxation time, as functions of polymer concentration; (c) effect of electrolyte viscosity on the width of the diffusion-limited regime in Zn||Zn and Zn||Nafion cells in the gravity stable configuration.

to be minimized. To understand the effect of gravity, the measurements were performed using cells in which the electric and gravitational fields are both antiparallel (stable) and parallel (unstable).

EXPERIMENTAL SECTION

We performed current−voltage ($J-V$) measurements for Zn||Zn symmetric and Zn||Nafion asymmetric electrochemical cells at 25 °C using a MACCOR battery tester. The cell configuration is reported in Figure S1. Aqueous viscoelastic electrolytes containing 50 mM $ZnSO_4$ were prepared by dissolving ultrahigh molecular weight ($M_w = 8 \times 10^6$ g/mol) polyethylene oxide (PEO) at concentrations ranging from 0 to 4 wt % in these electrolytes. The voltage step-ramp protocol depicted in Figure 1a was used for the $J-V$ measurements. As noted in the previous section, an important feature of the measurements is that by recording the current at long tines after the ramp-up in the respective voltage, the protocol ensures that the diffusion layer thickness is larger than the interelectrode spacing. Measurements were performed in both the gravity stable and unstable configurations to independently assess the role played by gravity-induced salt gradients on the $J-V$ curves.

RESULTS AND DISCUSSION

In the absence of the high molar mass polymer, results in Figure 1b show that at voltages above approximately 50 mV (i.e., ~2 kT/e), the current density in a Zn||Zn symmetric cell rises rapidly with voltage, exhibit large run-to-run variability (error bars), and the diffusion limit predicted when convection is ignored in classical Nernst−Planck (N−P) theory[1] is not observed in the gravity unstable configuration. In contrast, in the gravitationally stable case, a diffusion limiting current ($J_L \approx$ 2.4 mA/cm^2) is observed over a range of voltages (0.2−0.35 V; i.e. 7.9 kT/e to 13.8 kT/e). Both the voltage value at the onset of the diffusion limited regime, V_0, and the value of the limiting current recorded in the gravity stable configuration are close to the corresponding theoretical values ($V_0 \approx 8$ kT/e) and limiting current $J_{Theo} \approx$ 2.8 mA/cm^2, estimated using the classical theory and based on the electrolyte conductivity and cell geometry used in the study (eq S1). However, as shown in Figure 1b, when voltages higher than approximately 14 kT/e are applied to cells without polymer additive and in the gravity stable orientation, the current density rises above the limiting value and thereafter increases rapidly with voltage; quickly exceeding the current measurement limit of the equipment. The current increase is accompanied by large run-to-run variations (see size of error bars), comparable to those observed in Zn||Zn cells in the gravity unstable configuration.

The latter behavior is qualitatively similar to the over-limiting conductance region reported in previous experimental[23,24] and numerical simulation[25] studies. Comparison of the $J-V$ curves for the control and polymer-containing electrolytes in Figure 1b shows that the polymer substantially changes the shape of the curve for both cell configurations, with the more dramatic changes observed for cells in the gravity unstable configuration. It is remarkable that even at concentrations as low as 0.5 wt% the voltage range where a limiting current is observed is substantially enlarged. We note further that for cells in the gravity unstable configuration, the polymer additive also produces an obvious enlargement of the limiting current to a value of approximately 4.4 mA/cm^2; a nearly 75% increase relative to $J_{L,Theo}$. As remarkable as the effect of the added polymer is the fact that further increases in the PEO concentration above 0.5 wt% results in relatively small changes in the width of the diffusion limited transport regime (see Figure 1d and also Figure S2), even while measurably increasing the electrolyte viscosity (Figure 2a) and lowering the limiting current to values comparable to $J_{L,Theo}$.

In an initial attempt to simultaneously understand the effect of polymer and gravity on the measured $J-V$ curves, we computed the Rayleigh number for electrolytes with and without polymer. Table S1 shows that for the interelectrode spacing of 0.8 mm used for the studies reported in Figure 1b−d, R_a ranges from 5.9×10^5 (0 wt %, PEO), 7.7×10^3 (0.5 wt %), 10^5 (1 wt %), and 12 (2 wt %). The large R_a for the control (PEO-free) electrolytes is consistent with the large differences in $J-V$ curves observed for the gravity unstable cell orientation, indicating that gravity alone can produce large enhancements in the ion flux by a Rayleigh−Bernard-type convection mechanism discussed in previous work.[26]

Addition of polymer dramatically lowers Ra, suggesting that the polymer additive is able to eliminate gravity-assisted convection, explaining the recovery of classical N−P behaviors upon polymer addition. We note further that the polymer effects are similarly strong in cells in the gravity stable orientation, where the hydrodynamic stability termed electro-convection is considered responsible for the large increases in J.[25,27] On this basis, we conclude that relatively small amounts of PEO are effective in suppressing/eliminating convective flow in electrochemical cells, irrespective of the source.

Earlier studies by West[28,29] and Akoklar[13,14] have shown that polymer additives can profoundly influence deposition of metals such as Cu and Zn at planar substrates either by forming complexes with the metal ions to facilitate nucleation and regulate growth of the metal deposit or by absorbing to the deposit tips to suppress growth. A shortcoming of the results reported in Figure 1b is that it is impossible to separate specific surface effects associated with the metal deposition from any role the polymer might play in the electrokinetics. In other words, as hydrodynamic and morphological features associated

https://dx.doi.org/10.1021/acs.macromol.0c00037
Macromolecules 2020, 53, 2694−2701

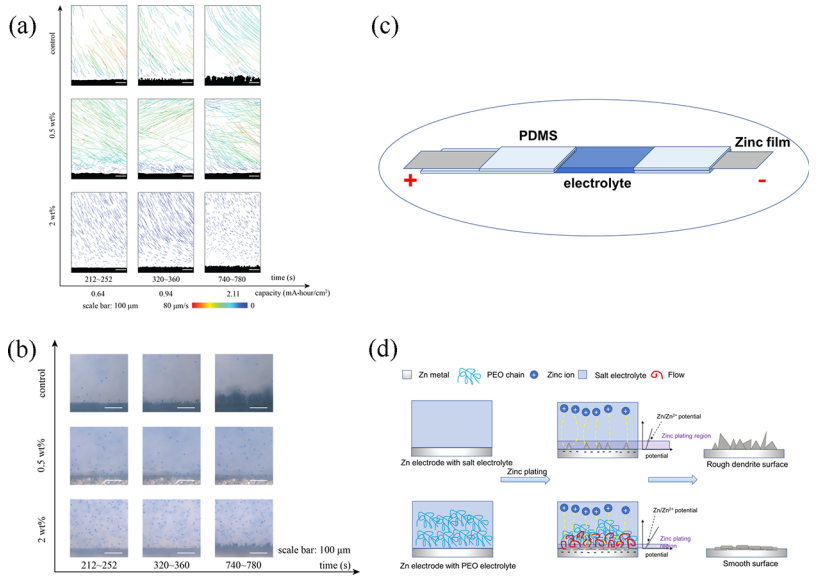

Figure 3. Visualizing electrolyte flow and electrode morphological evolution in Zn||Zn cells driven galvanostatically at 15 mA/cm^2. (a) Evolution of tracer particle trajectory and electrode surface morphology in control and $M_w = 8 \times 10^6$ g/mol PEO-enriched electrolytes. (b) Snapshots of particle trajectories and electrode surface morphology. (c) Zn||Zn visualization cell design used in the study. The interelectrode distance is 10 mm. (d) Illustration of mechanism through which polymer additives reduce electroconvection and smooth electrodeposition of Zn.

with the metal deposition reactions occur simultaneously in the Zn||Zn cells, fundamental understanding of the role played by the high molar mass polymer is not possible. In order to rule out effects associated with the changing metal interface produced by electrodeposition, we performed similar experiments employing a 50 μm thick cation selective Nafion membrane near the Zn surface. The membrane pretreated with a $ZnSO_4$ aqueous electrolyte is used to create an ion-selective interlayer in the Zn||Zn cells (Figure S1). The $J-V$ data reported in Figure 1c show that the gravity unstable cell orientation supports much larger ion fluxes and a diffusion-limited transport regime is again not observed. In contrast, a diffusion-limited regime is clearly apparent in the gravity stable configuration and the regime spans a moderately wider voltage range, 0.1−0.5 V (0.2−0.5 V; i.e. 16 kT/e to 20.5 kT/e), in comparison to the Zn||Zn cells. We note, however, that the limiting current remains approximately the same.

The corresponding effects of PEO additives on the $J-V$ curve in Zn||Zn cells that utilize the Nafion interlayer are reported in Figure 1c. Again, it is seen that addition of as little as 0.5 wt % PEO to the electrolyte produces both a large increase in the diffusion-limited transport regime and a large enhancement of J_L. One can rule out the potential trivial effect of the Nafion membrane in enhancing the overall concentration of mobile Zn ions in the electrolyte by calculating the maximum change in Zn^{2+} concentration if all of the sulfonate sites on Nafion are considered sources for Zn^{2+}. This calculation shows that the Zn^{2+} ions associated with the 50 μm Nafion membrane would increase the Zn^{2+} concentration in the electrolyte by at most 8%. On this basis, we conclude that the enhancement in J_L arises from a similar polymer-mediated source as for the Zn||Zn cells that does not require specific adsorption of polymer chains to a metal substrate. Additionally, as with the experiments performed in simple Zn||Zn cells, it is apparent that the enhancements in J_L are largest at small PEO concentrations and the effect quickly saturates with the PEO content (see Figure 1d). Again, we note the saturation is insensitive to whether the cells are held in the gravitationally stable or unstable orientations, but that the diffusion limited regime is consistently wider for the cells that employed the Nafion interlayer.

The results in Figure 1 therefore imply that the high molar mass PEO additive is effective in arresting overlimiting conductance, irrespective of its source, but the polymer is more effective in the case where the possibility of morphological instability is removed. Previous work[23] showed that the extension ΔV of the diffusion limited regime produced by polymer additives in carbonate electrolytes in Li||Li cells scales with electrolyte viscosity as $\Delta V \approx \sqrt{\mu}$ at low polymer concentration, and transitions to a weaker dependence, $\Delta V \approx \sqrt[4]{\mu}$ at higher polymer concentrations. The effect of PEO concentration on electrolyte viscosity and ionic conductivity are reported in Figure 2a. An increase in PEO concentration from 0 to 0.5 wt % produces a viscosity increment of 10^2, but only a 0.024% reduction in conductivity (Figure 2b). These observations are consistent with earlier reports,[23,24] which attribute the larger effect of polymer concentration on viscosity than on ionic mobility to the relative ease with which solvated ions can move through an entangled polymer network formed by ultrahigh molecular weight flexible polymer chains. The reports imply that over the range of PEO concentration studied in the present work, the electrolytes can be considered semidilute entangled polymer solutions. Figure 2c compares the normalized ΔV versus μ for all systems used in the study. The results are again consistent with previous work[23,24] and confirms that above a certain critical polymer concentration, the effectiveness of high molar mass polymer in delaying the onset of over-limiting conductance is limited.

The rheological properties of the electrolytes were investigated in small-amplitude oscillatory shear, and the results are reported in Figure S3a. We observe that however, the loss modulus G'' is larger than the storage modulus G' for the electrolyte containing 0.5 wt % PEO, and above 1 wt % PEO G' becomes dominant. The ratio of $G''$to G' reported in Figure S3b confirms that electrolytes transition from a viscous

https://dx.doi.org/10.1021/acs.macromol.0c00037
Macromolecules 2020, 53, 2694−2701

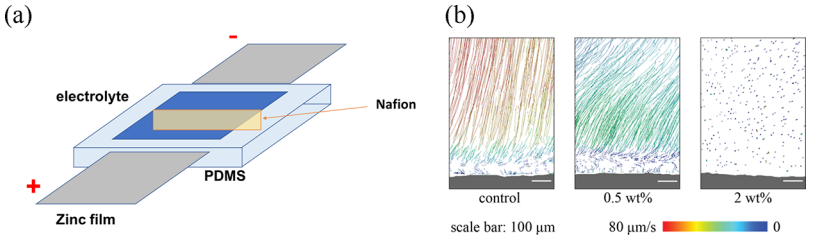

Figure 4. (a) Visualization cell design with Nafion. (b) Electroconvection in viscoelastic polymer electrolyte at ion selective Nafion membrane surface.

liquid-like response ($G''/G' > 1$), to a more solid elastic like response ($G''/G' < 1$) for PEO concentrations above 1 wt %. The entanglement molecular weight M_{e0} for a PEO melt has been reported to be approximately 1620 g/mol;[30] the onset of entanglement effects in an $M_w = 8 \times 10^6$ g/mol PEO solution would therefore be expected at a polymer volume fraction, $\phi_{e,PEO} = \left(\frac{M_w}{2 \times M_{e0}}\right)^{-3/4} \approx 2.86 \times 10^{-3}$. For the aqueous electrolytes used in the study, this corresponds to a polymer concentration of approximately 0.3 wt %, which is comparable to the PEO concentration at which the transition to elasticity dominant fluid rheology is observed. The mesh size of the entanglement network can also be estimated from the measured elastic modulus in the linear viscoelastic regime to lie in the range of 22−196 nm as the polymer concentration is lowered. These values are evidently quite a bit larger than the estimated size of a hydrated Zn^{2+} ionic radii (0.21−0.24 nm[31,32]), which would explain why the electrolytes are able to simultaneously exhibit liquid-like ion mobilities but strong resistance to electrolyte convection in either the stable or unstable cell orientations.

We fabricated an optical visualization cell (Figure 3c) that can be mounted between the sample stage and objective of an optical microscope (Olympus) outfitted long working distance objective. To visualize transport processes in the cells, 10 μm uncharged polystyrene microparticles dyed blue were dispersed in the electrolytes and used as fluid tracers to track time- and space-resolved dynamics in the electrolyte near Zn electrodes and Nafion interlayers. By performing experiments in electrolytes with and without polymer additives, it is possible to unambiguously interrogate convective processes in the cells and to more precisely establish the role the polymers play in extending the diffusion-limited transport regime. An additional benefit of the visualization experiments is that because morphological changes at a Zn metal electrode can be studied at the same time as the tracer particle trajectories, comparison of particle trajectories near the Zn and cation-selective Nafion membrane can be used to isolate purely hydrodynamic from morphology and hydrodynamic effects on the electrolyte velocity field. For simplicity, the visualization experiments were performed at a constant current of 15 mA/cm^2 and at room temperature.

Figures 3a,b and S4 report tracer particle trajectories and snapshots, respectively, in the Zn||Zn cells in electrolytes in which the PEO polymer is present at different concentrations. It is immediately apparent that strong convective processes are present in the control (no PEO) electrolytes and overtime, obvious dendritic deposits form at the Zn electrode. In the electrolyte containing only 0.5 wt % PEO, the particle motions are noticeably slowed, especially obvious at the surface, with fewer "hot spots" (i.e., regions where the tracer velocity are highest, see Figure S4) than in the control case. The results therefore establish that the polymer stabilizes the electroconvective instability, producing a more uniform flux to the electrode. Inspection of the Zn electrode morphology reveals more uniform deposition and no obvious dendrite formation during the experimental period. Both observations are consistent with recent numerical simulations,[25] which show that polymer stretching due to the high-curvature, localized eddies formed at the electrode surface facilitates mixing in the ESCL to produce a more uniform ion flux to the Zn metal electrode (see Figure 3d). The results show further that a higher polymer concentration is not necessarily good. While the average tracer particle velocity is noticeably lower (see Figure S4) in more viscous electrolytes containing 2 wt % PEO, Zn dendrites reappear at long run times. The analogous results from tracer visualization studies in electrolytes near the cation-selective Nafion membrane are reported in Figure 4a. The measurements again show that strong convective flow occurs in the control electrolyte and that the convection results in accelerated tracer particle motion toward the electrode with the strongest flow occurring at distances of 100 μm or more away from the electrode.

Within this 100 μm boundary layer, a strongly swirling three-dimensional flow comprised of transient rolls/eddies is observed. The structure of this flow, including the appearance of the eddies in counterrotating pairs, is strikingly similar to convective flows predicted by direct numerical simulations[25] to accompany electroconvective hydrodynamic instability in closed electrochemical cells. We note however that the thickness of the boundary layer is more than 10 times larger than the extended space-charge layer thickness, $\Lambda_{ESCL} \approx L\left\{\left(\frac{Ve}{kT}\right)\frac{\kappa^{-1}}{L}\right\}^{2/3} = 1 - 10\,\mu$m predicted both by theory[33] and estimated from numerical simulations[25] for the salt concentration, voltage, and interelectrode spacing used in the present study. Thus, the boundary layer so clearly observed in the experiments defies any simple comparisons with the ESCL proposed in current theories for *second-kind* electroosmotic slip as the source of electroconvection near a cation selective membrane.

As was the case for visualization experiments near a metallic Zn electrode, we note further that addition of 0.5 wt % PEO to the electrolyte dramatically reduces the average velocity of the flow and eliminates local regions of high velocity. Importantly, however, the thickness of the boundary layer is essentially unchanged. In contrast, for the more viscous electrolyte (2 wt % PEO), both the flow velocity and thickness of the boundary layer are systematically lowered (see Figures 4b and S5); and no obvious convective rolls are observed. The results imply that at higher polymer concentration, electroconvection is more completely suppressed in the electrolytes near cation-

https://dx.doi.org/10.1021/acs.macromol.0c00037
Macromolecules 2020, 53, 2694−2701

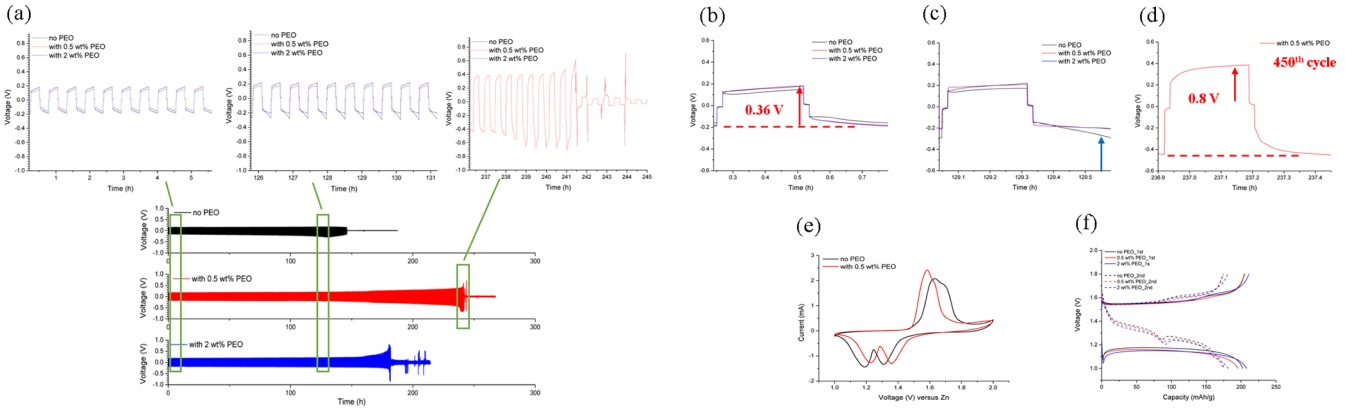

Figure 5. (a) Zn|Zn symmetric galvanostatic cycling, 1 mA/cm^2, 0.25 mA h/cm^2, (b) 1st cycle, (c) 242nd cycle, (d) 450th cycle electrochemical behavior of Zn−MnO_2 batteries with salt and polymer electrolyte (e) comparison of CV scanning at 0.1 mV/s, second cycle. (f) Charge/discharge curve Zn/MnO_2 battery in the initial and second cycle.

selective membranes than near a metal electrode. This observation simultaneously explains the larger effect of polymer additives in extending the diffusion-limited transport regime for cells containing the Nafion interlayer and indicates that the coupling between the morphological and hydrodynamic instability near a metal electrode may mitigate some of the benefits of the polymer additive.

Previous studies have shown that low molecular weight PEO can serve as a *leveler* during electrodeposition of Cu but that the effect results from complexation of copper ions and PEO chains in solution and adsorption of PEO on the reduced copper metal at the electrode.[28,29] Similar effects are in principle possible for the Zn|Zn case[13,14] but are unlikely to play a role in the Zn|Nafion systems used in the study. To understand the role of polymer adsorption on the observations reported in Figure 1a,d and 3, we employed X-ray photoelectron spectroscopy (XPS, SSX-100) and Fourier-transform infrared spectroscopy (FTIR, Thermo Scientific) to interrogate the surface of the Zn working electrode after the visualization studies. These electrodes were first washed with chloroform and then deionized water to remove electrolyte and loosely bonded polymers. Comparison of the binding energies from the measured XPS spectra in the control electrolytes with values reported in the literature, Figure S6 and Table S3,[34−38] indicate that either ZnO or $Zn(OH)_2$ is the dominant component on the Zn electrode. The Zn $2p_{3/2}$ binding energy for Zn electrodes harvested from the PEO-containing electrolyte also indicate the formation of ZnO or/and $Zn(OH)_2$.[38−41] An oxygen binding energy peak at ∼531 eV is attributed to $ZnCO_3$ formation, likely originating from atmospheric exposure of the samples, and the peak at 529.39 eV indicates the ZnO formation.[42] The results do show a somewhat weaker contribution at 284.5 eV that can be assigned to C−C groups, and a secondary peak at 288 eV, which is associated with C−O−C groups,[43] implying that some level of polymer adsorption occurs.

On surfaces interacting with either the control or polymer electrolytes, we detect similar FTIR peak patterns, Figure S7. The presence of an IR vibration band at 3476 cm^{-1} is tentatively assigned to the stretching vibration of intermolecular hydrogen bonds (OH) associated with absorbed water on the electrode surface. We note nonetheless that zinc oxide has a IR band in the range 3620−2950 cm^{-1}.[38−40] The FTIR spectra also shows a broad peak 1236−500 cm^{-1} which can be assigned to the metal−oxygen (Zn−O) bonds of ZnO, which are typically in the range 680 to 300 cm^{-1}.[38,40] Furthermore, literature reports[41] indicate that PEO absorbed on ZnO will produce IR peaks in the region of 1511 and 1394 cm^{-1}, which are not seen in our systems. Additionally, comparing the measured spectra to that of the pure PEO powder, the FTIR results do not support a strongly adsorbed PEO layer on the Zn electrode. Thus, we conclude, that the strong PEO surface adsorption effects reported for Cu are perhaps less important for the Zn systems studied here.

To evaluate the practical benefits of high molecular weight PEO electrolyte additives in battery cells that used Zn anodes, we investigate the reversibility of Zn metal electrodes in symmetric Zn|Zn symmetric cells in galvanostatic cycling (Figure 5a−d) by the Battery Testing System (Neware) at 25 °C. The measurements were performed at a current density 1 mA/cm^2 and for a fixed capacity of 0.25 mA h/cm^2. The cell setup is shown in Figure S1a, and the electric field lies orthogonally to the gravity direction. Initially, the PEO-containing electrolyte shows a slightly higher polarization, compared to the control aqueous electrolyte, possibly due to an increase in the interfacial resistance by the low concentration of PEO. After 200 cycles, both the Ohmic and concentration polarization of control aqueous electrolyte increases, which likely indicates an increased energy barrier for metal nucleation and less uniform metal deposition. This inference is supported by the fact that the cells suddenly fail at around 145 h due to metal-induced short circuits.[44]

In comparison, the cells containing the PEO polymer electrolyte additive remain stable for more than 225 h. Interestingly, consistent with the results reported in Figure 3a,b, we find that cells containing 0.5 wt % PEO electrolyte exhibit greater stability than those containing higher concentrations of the polymer. Motivated by these observations, we created full Zn−MnO_2 battery cells (Figure S1c) and evaluated the effect of PEO additives on their performance. In cyclic voltammetry (CV) measured by Electrochemical Analyzer (CH Instruments, Inc.) at room temperature in Figure 5e the reduction reaction from MnO_2 to soluble Mn^{2+} is seen to be a two electron process, occurring at 1.35 and 1.2 V versus Zn^{2+}/Zn. The oxidation reaction from Mn^{2+} to MnO_2 occurs at 1.6 V versus Zn^{2+}/Zn. The pairs of redox peaks correspond to the two plateaus in the charge−discharge curves, Figure 5f, where the charge and discharge for the initial two

https://dx.doi.org/10.1021/acs.macromol.0c00037
Macromolecules 2020, 53, 2694−2701

cycles of Zinc/MnO_2 battery shows different curves. This is due to the conversion reaction mechanism where α-MnO_2 structure and morphology evolve after the initial cycle, which benefits electrode structural mechanics and kinetics while increases the surface energy.[18] CV measurements further show that the redox reactions at the Zn electrode are unaffected by the presence of PEO in the electrolyte. In the scan from low to high voltage at 0.1 mV/s, the peak cathodic current of PEO electrolyte shifts to a lower voltage with a higher current value, indicating the faster delivery of additional ions from the bulk solution to the electrode, which is consistent with the previous observation of mixing effect in 0.5 wt % PEO electrolyte. For the same reason, during the reserve scan, the anodic peak shifts to a higher voltage. In the charge/discharge process, their performance is similar, showing good rate capacity at 2.6C, and high reversible capacity is delivered in the first and second cycles, close to the reported high reversible capacity.[18] The zinc electrode morphology after cycles was characterized by a scanning electron microscope (Keck) (Figure S8). Smooth flake-like deposits on micrometer scales are observed, indicating that in the 0.5 wt % PEO electrolyte the polymer has a beneficial effect in stabilizing Zn electrodeposition.

CONCLUSIONS

Introducing a small amount of ultrahigh molecular weight PEO in an aqueous liquidelectrolyte is shown to to be highly effective in improving the stability of ion transport and electrodeposition at ion-selective interfaces. We find that the effectiveness of high molar mass polymers mainly result from their ability to produce large increases in solution viscosity, without slowing down ion migration rates. The resultant electrolytes therefore exhibit a combination of polymer-like viscoelastic properties and liquid-like fast ion transport that allows them to actively suppress electroconvection. It is also reported that the inter-electrode distance plays an important role in inducing electroconvection, but that the polymer concentration in an electrolyte is easily able to overcome these effects to enhance stability of electrodeposition in both gravitational stable and unstable configurations. PEO is chemically stable during the electrochemical reaction occurring on the zinc electrodes, and 0.5 wt % PEO has preferred rheological properties to introduce local flow, facilitating efficient mixing in the space charge layer scale, which also enhance the Zn/MnO_2 battery performance. This shines light on that using small amount of high molecular weight PEO in the mild aqueous electrolyte is promising to produce high performance and environmentally friendly zinc-based energy storage at low cost. It also opens up opportunities for creating novel electrolytes using long-chain branched[45,46] and other architecturally complex polymer additives able to generate elasticity-driven secondary flows that may suppress electroconvection in liquid electrolytes at even lower polymer concentrations.

ASSOCIATED CONTENT

Supporting Information

The Supporting Information is available free of charge at https://pubs.acs.org/doi/10.1021/acs.macromol.0c00037.

Materials used in the study, analytical methods, and additional data (PDF)

AUTHOR INFORMATION

Corresponding Author

Lynden A. Archer − *School of Chemical and Biomolecular Engineering, Cornell University, Ithaca, New York 14853, United States;* orcid.org/0000-0001-9032-2772; Email: laa25@cornell.edu

Authors

Duhan Zhang − *School of Mechanical and Aerospace Engineering, Cornell University, Ithaca, New York 14853, United States;* orcid.org/0000-0001-9428-956X

Alexander J. Warren − *School of Chemical and Biomolecular Engineering, Cornell University, Ithaca, New York 14853, United States*

Gaojin Li − *School of Chemical and Biomolecular Engineering, Cornell University, Ithaca, New York 14853, United States*

Zhu Cheng − *School of Chemical and Biomolecular Engineering, Cornell University, Ithaca, New York 14853, United States*

Xiaoxing Han − *School of Chemical and Biomolecular Engineering, Cornell University, Ithaca, New York 14853, United States*

Qing Zhao − *School of Chemical and Biomolecular Engineering, Cornell University, Ithaca, New York 14853, United States*

Xiaotun Liu − *School of Chemical and Biomolecular Engineering, Cornell University, Ithaca, New York 14853, United States*

Yue Deng − *School of Materials Science and Engineering, Cornell University, Ithaca, New York 14853, United States*

Complete contact information is available at: https://pubs.acs.org/10.1021/acs.macromol.0c00037

Notes

The authors declare no competing financial interest.

ACKNOWLEDGMENTS

This research is supported by Department of Energy Basic Energy Science Program through Grant DE-SC0016082. Technical and facility support provided by the Cornell Energy Systems Institute (CESI) are also gratefully acknowledged. This work made use of the Cornell Center for Materials Research Shared Facilities which are supported through the NSF MRSEC program (DMR-1719875).

REFERENCES

(1) Newman, J.; Thomas-Alyea, K. E. *Electrochemical Systems*; John Wiley & Sons, 2012.

(2) Rubinstein, I.; Zaltzman, B. Dynamics of extended space charge in concentration polarization. *Phys. Rev. E* **2010**, *81*, 061502.

(3) Ward, W. J.; Le Blanc, O. H. Rayleigh-Benard Convection in an Electrochemical Redox Cell. *Science* **1984**, *225*, 1471−1473.

(4) De Valença, J. C.; Kurniawan, A.; Wagterveld, R. M.; Wood, J. A.; Lammertink, R. G. Influence of Rayleigh-Bénard convection on electrokinetic instability in overlimiting current conditions. *Phys. Rev. Fluids* **2017**, *2*, 033701.

(5) Volgin, V. M.; Davydov, A. D. Natural-convective instability of electrochemical systems: A review. *Russian J. Electrochem.* **2006**, *42*, 567−608.

(6) Baranowski, B.; Kawczyński, A. L. Experimental determination of the critical Rayleigh number in electrolyte solutions with concentration polarization. *Electrochim. Acta* **1972**, *17*, 695−699.

(7) Liu, M.; Yang, L.; Liu, H.; Amine, A.; Zhao, Q.; Song, Y.; Yang, J.; Wang, K.; Pan, F. Artificial Solid-Electrolyte Interface Facilitating Dendrite-Free Zinc Metal Anodes via Nanowetting Effect. *ACS Appl. Mater. Interfaces* **2019**, *11*, 32046−32051.

(8) Karatay, E.; Andersen, M. B.; Wessling, M.; Mani, A. Coupling between buoyancy forces and electroconvective instability near ion-selective surfaces. *Phys. Rev. Lett.* **2016**, *116*, 194501.
(9) Pan, J.; Xu, Y. Y.; Yang, H.; Dong, Z.; Liu, H.; Xia, B. Y. Advanced Architectures and Relatives of Air Electrodes in Zn-Air Batteries. *Adv. Sci.* **2018**, *5*, 1700691.
(10) Mainar, A.; Colmenares, L.; Grande, H.-J.; Blázquez, J. Enhancing the Cycle Life of a Zinc-Air Battery by Means of Electrolyte Additives and Zinc Surface Protection. *Batteries* **2018**, *4*, 46−64.
(11) Barton, J. L.; Bockris, J. O'M. The electrolytic growth of dendrites from ionic solutions. *Proc. Royal Society* **1962**, *A2668*, 485−505.
(12) Oren, Y.; Landau, U. Growth of Zinc Dendrites in Acidic Zinc Chloride Solutions. *Electrochim. Acta* **1982**, *27*, 739−748.
(13) Banik, S. J.; Akolkar, R. Suppressing Dendrite Growth during Zinc Electrodeposition by PEG-200 Additive. *J. Electrochem. Soc.* **2013**, *160*, D519−D523.
(14) Banik, S. J.; Akolkar, R. Suppressing Dendritic Growth during Alkaline Zinc Electrodeposition using Polyethylenimine Additive. *Electrochim. Acta* **2015**, *179*, 475−481.
(15) Zheng, J.; Zhao, Q.; Tang, T.; Yin, J.; Quilty, C. D.; Renderos, G. D.; Liu, X.; Deng, Y.; Wang, L.; Bock, D. C.; Jaye, C.; Zhang, D.; Takeuchi, E. S.; Takeuchi, K. J.; Marschilok, A. C.; Archer, L. A. Reversible epitaxial electrodeposition of metals in battery anodes. *Science* **2019**, *366*, 645−648.
(16) Aubin, C. A.; Choudhury, S.; Jerch, R.; Archer, L. A.; Pikul, J. H.; Shepherd, R. F. Electrolytic vascular systems for energy-dense robots. *Nature* **2019**, *571*, 51−57.
(17) Xu, C.; Li, B.; Du, H.; Kang, F. Energetic Zinc Ion Chemistry: The Rechargeable Zinc Ion Battery. *Angew. Chem., Int. Ed.* **2012**, *51*, 933−935.
(18) Pan, H.; Shao, Y.; Yan, P.; Cheng, Y.; Han, K. S.; Nie, Z.; Mueller, K. T. Reversible aqueous zinc/manganese oxide energy storage from conversion reactions. *Nature Energy* **2016**, *1*, 16039.
(19) Zhang, N.; Cheng, F.; Liu, Y.; Zhao, Q.; Lei, K.; Chen, C.; Liu, X.; Chen, J. Cation-Deficient Spinel ZnMn2O4 Cathode in Zn(CF3SO3)2 Electrolyte for Rechargeable Aqueous Zn-Ion Battery. *J. Am. Chem. Soc.* **2016**, *138*, 12894−12901.
(20) Parker, J. F.; Chervin, C. N.; Pala, I. R.; Machler, M.; Burz, M. F.; Long, J. W.; Rolison, D. R. Rechargeable nickel-3D zinc batteries: An energy-dense, safer alternative to lithium-ion. *Science* **2017**, *356*, 415−418.
(21) Gallaway, J. W.; Desai, D.; Gaikwad, A.; Corredor, C.; Banerjee, S.; Steingart, D. A lateral microfluidic cell for imaging electro-deposited zinc near the shorting condition. *J. Electrochem. Soc.* **2010**, *157*, A1279−A1286.
(22) Kang, L.; Cui, M.; Jiang, F.; Gao, Y.; Luo, H.; Liu, J.; Liang, W.; Zhi, C. Nanoporous CaCO3 Coatings Enabled Uniform Zn Stripping/Plating for Long-Life Zinc Rechargeable Aqueous Batteries. *Adv. Energy Mater.* **2018**, *8*, 1801090.
(23) Wei, S.; Cheng, Z.; Nath, P.; Tikekar, M. D.; Li, G.; Archer, L. A. Stabilizing electrochemical interfaces in viscoelastic liquid electrolytes. *Sci. Adv.* **2018**, *4*, No. eaao6243.
(24) Warren, A.; Zhang, D.; Choudhury, S.; Archer, L. A. Electrokinetics in viscoelastic liquid electrolytes above the diffusion limit. *Macromolecules* **2019**, *52*, 4666−4672.
(25) Li, G.; Archer, L. A.; Koch, D. L. Electroconvection in a viscoelastic electrolyte. *Phys. Rev. Lett.* **2019**, *122*, 124501.
(26) Karatay, E.; Andersen, M. B.; Wessling, M.; Mani, A. Coupling between buoyancy forces and electroconvective instability near ion-selective surfaces. *Phys. Rev. Lett.* **2016**, *116*, 194501.
(27) Tikekar, M. D.; Li, G.; Archer, L. A.; Koch, D. L. Electroconvection and Morphological Instabilities in Potentiostatic Electrodeposition across Liquid Electrolytes with Polymer Additives. *J. Electrochem. Soc.* **2018**, *165*, A3697−A3713.
(28) Kelly, J. J.; West, A. C. Copper Deposition in the Presence of Polyethylene Glycol. *J. Electrochem. Soc.* **1998**, *145*, 3472−3476.
(29) Kelly, J. J.; West, A. C. Copper Deposition in the Presence of Polyethylene Glycol. *J. Electrochem. Soc.* **1998**, *145*, 3477−3481.
(30) Zardalidis, G.; Mars, J.; Allgaier, J.; Mezger, M.; Richter, D.; Floudas, G. Influence of chain topology on polymer crystallization: poly(ethylene oxide) (PEO) rings vs. linear chains. *Soft Matter* **2016**, *12*, 8124−8134.
(31) Musinu, A.; Paschina, G.; Piccaluga, G.; Magini, M. The sulphate ion in aqueous solution: an X-ray diffraction study of a ZnSO4solution. *J. Appl. Crystallogr.* **1982**, *15*, 621−625.
(32) Vlaev, L. T.; Georgieva, V. G.; Genieva, S. D. Kinetic parameters of decomposition of some selenites. *J. Therm. Anal. Calorim.* **2006**, *83*, 421−427.
(33) Chazalviel, J.-N. Electrochemical aspects of the generation of ramified metallic electrodeposits. *Phys. Rev. A* **1990**, *42*, 7355.
(34) Dake, L. S.; Baer, D. R.; Zachara, J. M. Auger parameter measurements of zinc compounds relevant to zinc transport in the environment. *Surf. Interface Anal.* **1989**, *14*, 71−75.
(35) Fürbeth, W.; Stratmann, M. The delamination of polymeric coatings from electrogalvanised steel - a mechanistic approach. *Corros. Sci.* **2001**, *43*, 207−227.
(36) Biesinger, M. C.; Lau, L. W. M.; Gerson, A. R.; Smart, R. S. C. Resolving surface chemical states in XPS analysis of first row transition metals, oxides and hydroxides: Sc, Ti, V, Cu and Zn. *Appl. Surf. Sci.* **2010**, *257*, 887−898.
(37) Bera, S.; Dhara, S.; Velmurugan, S.; Tyagi, A. K. Analysis on binding energy and auger parameter for estimating size and stoichiometry of ZnO nanorods. *Int. J. Spectrosc.* **2012**, *2012*, 371092.
(38) Winiarski, J.; Tylus, W.; Winiarska, K.; Szczygieł, I.; Szczygieł, B. XPS and FT-IR Characterization of Selected Synthetic Corrosion Products of Zinc Expected in Neutral Environment Containing Chloride Ions. *J. Spectrosc.* **2018**, *2018*, 2079278.
(39) Moulder, J. F. *Handbook of X-ray Photoelectron Spectroscopy*; Perkin-Elmer Corporation, 1995; pp 230−232.
(40) Kajbafvala, A.; Zanganeh, S.; Kajbafvala, E.; Zargar, H. R.; Bayati, M. R.; Sadrnezhaad, S. K. Microwave-assisted synthesis of narcis-like zinc oxide nanostructures. *J. Alloys Compd.* **2010**, *497*, 325−329.
(41) Liufu, S.; Xiao, H.; Li, Y. Investigation of PEG adsorption on the surface of zinc oxide nanoparticles. *Powder Technol.* **2004**, *145*, 20−24.
(42) Duchoslav, J.; Steinberger, R.; Arndt, M.; Stifter, D. XPS study of zinc hydroxide as a potential corrosion product of zinc: Rapid X-ray induced conversion into zinc oxide. *Corros. Sci.* **2014**, *82*, 356−361.
(43) Greczynski, G.; Hultman, L. C 1s peak of adventitious carbon aligns to the vacuum level: dire consequences for material's bonding assignment by photoelectron spectroscopy. *ChemPhysChem* **2017**, *18*, 1507−1512.
(44) Zhang, R.; Chen, X.-R.; Chen, X.; Cheng, X.-B.; Zhang, X.-Q.; Yan, C.; Zhang, Q. Lithiophilic Sites in Doped Graphene Guide Uniform Lithium Nucleation for Dendrite-Free Lithium Metal Anodes. *Angew. Chem., Int. Ed.* **2017**, *56*, 7682.
(45) Archer, L. A.; Juliani. Linear and nonlinear viscoelasticity of entangled multiarm (pom-pom) polymer liquids. *Macromolecules* **2004**, *37*, 1076−1088.
(46) Archer, L. A.; Varshney, S. K. Synthesis and relaxation dynamics of multiarm polybutadiene melts. *Macromolecules* **1998**, *31*, 6348−6355.

https://dx.doi.org/10.1021/acs.macromol.0c00037
Macromolecules 2020, 53, 2694−2701